Highly deformed band structures due to core excitations in math xmlns="http://www.w3.org/1998/Math/MathML">mmultiscripts>mi>Xe/mi>mprescripts>/mprescripts>none>/none>mn>123/mn>/mmultiscripts>/math>

Anwesha Basu, A. K. Singh, I. Ragnarsson, B. G. Carlsson, A. Kardan, G. B. Hagemann, G. Sletten, B. Herskind, H. Hübel, S. Chmel, A. N. Wilson, J. Rogers, R. V. F. Janssens, M. P. Carpenter, T. L. Khoo, F. G. Kondev, T. Lauritsen, S. Zhu, A. Korichi, P. Fallon, B. M. Nyakó, and J. Timár

Phys. Rev. C **103**, 014301 — Published 4 January 2021

DOI: 10.1103/PhysRevC.103.014301

Highly-deformed band structures due to core excitations in ^{123}Xe

Anwesha Basu and A. K. Singh
Department of Physics, Indian Institute of Technology Kharagpur, Kharagpur 721302, India

I. Ragnarsson and B. G. Carlsson
Division of Mathematical Physics, LTH, Lund University, Box 118, SE-221 00 Lund, Sweden

A. Kardan
School of Physics, Damghan University, P.O. Box 36716-41167, Damghan, Iran

G. B. Hagemann, G. Sletten, and B. Herskind
Niels Bohr Institute, Blegdamsvej 17, DK-2100 Copenhagen Ø, Denmark

H. Hübel and S. Chmel*
Helmholtz-Institut für Strahlen- und Kernphysik, Universität Bonn, Nussallee 14-16, D-53115 Bonn, Germany

A. N. Wilson† and J. Rogers
R. S. P. E., ANU, Canberra, ACT 0200, Australia

R. V. F. Janssens
Department of Physics and Astronomy, University of North Carolina at Chapel Hill, Chapel Hill, North Carolina 27599, USA and Triangle Universities Nuclear Laboratory, Duke University, Durham, North Carolina 27708, USA

M. P. Carpenter, T. L. Khoo, F. G. Kondev, T. Lauritsen, and S. Zhu
Physics Division, Argonne National Laboratory, Lemont, Illinois 60439, USA

A. Korichi
IJCLab-IN2P3/CNRS, F-91405 Orsay Campus, France

P. Fallon
Nuclear Science Division, Lawrence Berkeley National Laboratory, Berkeley, California 94720, USA

B. M. Nyakó and J. Timár
Institute for Nuclear Research (Atomki), P.O. Box 51, 4001 Debrecen, Hungary

High-spin states in ^{123}Xe were populated in the ^{80}Se(^{48}Ca, 5n)^{123}Xe reaction at a beam energy of 207 MeV. Gamma-ray coincidence events were recorded with the Gammasphere spectrometer. Four new high-spin bands have been discovered in this nucleus.The bands are compared with those calculated within the framework of cranked Nilsson-Strutinsky and cranked Nilsson-Strutinsky-Bogoliubov models. It is concluded that the configurations of the bands involve two-proton excitations across the $Z = 50$ as well as excitation of neutrons across the $N = 82$ shell gaps resulting in a large deformation, $\varepsilon_2 \approx 0.30$ and $\gamma \approx 5^\circ$.

PACS numbers:

Keywords: Nuclear reaction:^{80}Se(^{48}Ca,5n)^{123}Xe; E= 207 MeV; Measured $\gamma\gamma$-coincidences; E_γ; I_γ; R_θ ratios; ^{123}Xe deduced levels; spin and parity; cranked Nilsson-Strutinsky and cranked Nilsson-Strutinsky-Bogoliubov models calculation

I. INTRODUCTION

Angular momentum in atomic nuclei is generated by the alignment of individual nucleon spins. In nuclei with just a few nucleons outside a closed core, the angular momentum is generally built from the full alignment of a few spin vectors, creating an irregular energy level pattern, whereas in deformed nuclei, far off closed shells, the grad-

*Present address : Fraunhofer INT, Appelsgarten 2, D-53879 Euskirchen, Germany
†Present address : Faculty of Social Sciences, University of Stirling, Stirling FK9 4LA, UK

ual alignment of many spin vectors gives rise to collective rotation with regular band structures. The competition of these modes of excitation, in particular in the transitional regions between spherical and deformed nuclei, is of special interest [1, 2].

The nuclei in the A≈125 mass region are soft towards deformation changes. They lie in the transitional region between spherical (Sn) and deformed (Ce) nuclei. The interplay of a variety of shapes is observed here with the excitation of a few valence nucleons to deformation driving $h_{11/2}$ intruder orbitals which are accessible to both, protons and neutrons. At low spin values, these $h_{11/2}$ nucleons have opposite deformation-driving effects; the protons favor a prolate shape while the alignment of the neutrons drives the nucleus towards an oblate shape[3–5].

Shape changes from a weakly prolate shape to an oblate one at medium spin have been reported in several nuclei of this mass region [6–14]. With increasing rotational frequency, nucleon pairs are broken and the spin vectors are gradually aligned along the rotational axis, inducing shape changes, until the bands terminate in maximally aligned oblate states where all the valence particles outside the closed ^{114}Sn core ($Z = 50$, $N = 64$) are aligned. Thereafter, higher angular momentum states can only be generated in configurations involving single-particle excitations from the ^{114}Sn core across the shell gaps.

At high spin, collective rotation competes with non-collective excitations. Deformed rotational bands extending to spin ≈ 50-60 have been observed in the ^{124}Ba [7], ^{120,122}Te [9, 13], ^{123,125}I [15, 16], and ^{124,125,126}Xe [17–19] nuclei. These bands decay to the normal-deformed (ND) levels at around spin 20-25 and ≈10 MeV excitation energy. From lifetime measurements in ^{125,126}Xe [18, 19], transition quadrupole moments have been estimated to lie in the 4.3-5.9 eb range, corresponding to deformation parameters ε_2 between 0.27 and 0.36. These high-spin bands can only be generated in configurations involving core-breaking excitations [9, 13, 15, 17]. Configuration assignments, based on cranked Nilsson-Strutinsky (CNS) calculations, suggest that these bands are built from proton excitations across the $Z = 50$ shell gap, combined with either neutron excitations within the $N = 50 - 82$ shell or neutron excitations involving the $i_{13/2}$ and $f_{7/2}, h_{9/2}$ orbitals across the $N = 82$ shell gap [16–18].

In this article, we report on the observation of new rotational structures at high spin in ^{123}Xe. Four highly-deformed bands, with characteristics similar to those observed in $^{124-126}$Xe, have been observed to feed ND levels of ^{123}Xe [20]. Several decay branches have been observed to emerge at the bottom of the bands, feeding multiple medium-spin band structures. However, they could not be firmly placed in the level scheme due to their weak intensities. Tentative spin and parity assignments, along with the possible configurations of the bands, are discussed within the framework of the CNS and cranked Nilsson-Strutinsky-Bogoliubov (CNSB) models.

II. EXPERIMENTAL DETAILS AND ANALYSIS

High-spin states of ^{123}Xe were populated in a heavy-ion fusion evaporation reaction, ^{80}Se(^{48}Ca,5n)^{123}Xe, at the ATLAS accelerator of Argonne National Laboratory, USA. The ^{48}Ca beam of 207 MeV energy and 4 pnA current bombarded a target composed of a 0.6 mg/cm^2 thick layer of ^{80}Se evaporated on a 0.3 mg/cm^2 Au backing. A layer of Au, with a thickness of 0.04 mg/cm^2, protected the front of the Se target. The target was mounted on four segments of a rotating wheel. In addition, the beam was slightly defocused and wobbled to prevent heat damage of the target [11]. Gamma-ray coincidence events were recorded with the Gammasphere spectrometer [21] which consisted of 101 Compton-suppressed Ge detectors at the time of the experiment. Over a beam time of ten days, 2.7×10^9 events, with Ge-detector coincidence fold ≥ 4, were recorded by the spectrometer. Although the main motivation behind the experiment was to search for hyperdeformed structures in ^{124}Xe, high-spin states of ^{123}Xe were populated adequately to carry out the present study. The other dominant channels populated in this experiment were *4n, p4n*, and $\alpha 4n$ leading to ^{124}Xe [17], ^{123}I [11, 15], and ^{120}Te [13], respectively.

The raw data were calibrated and gain matched and were sorted into $\gamma - \gamma$ coincidence matrices, $\gamma - \gamma - \gamma$ cubes and $\gamma - \gamma - \gamma - \gamma$ hypercubes. The offline analysis was carried out with the help of the RADWARE software package [22]. Angular distribution matrices were produced to determine multipolarities of γ rays. Typical values of the angular distribution ratio R_θ, defined in Ref. [20], for stretched dipole and stretched quadrupole transitions lie around 0.6 and 1.4, respectively. The details of the measurement and data analysis are reported in an earlier publications on ^{123}Xe [20].

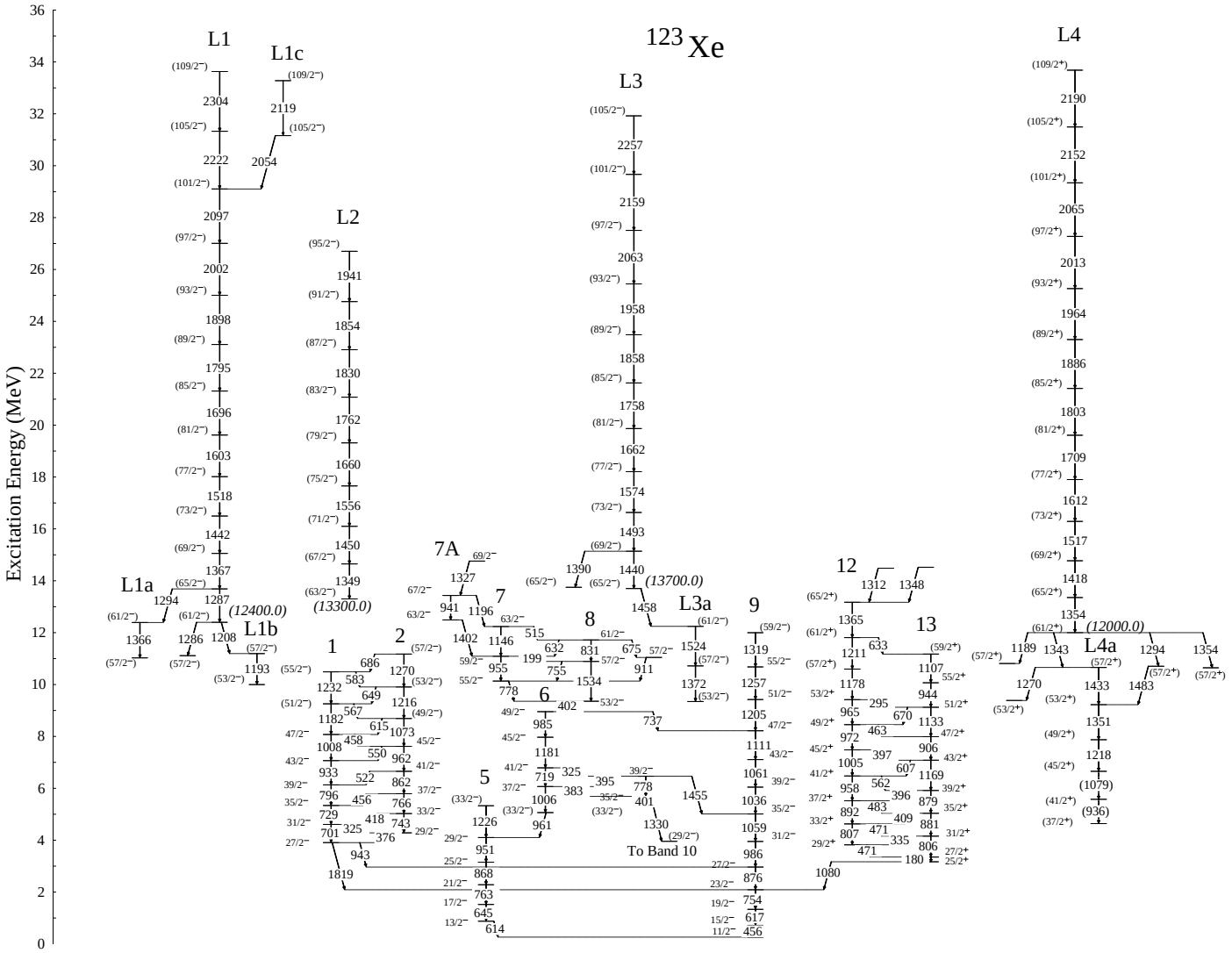

FIG. 1: Partial level scheme of ^{123}Xe showing the new high-spin bands L1-L4 described in the present work. The tentative level energies and spins of L1-L4 have been estimated from the patterns of their decays to ND levels (see text for details). The low-lying structures, numbered 1 to 13, are taken from Ref. [20].

TABLE I: Gamma-ray energies, tentative level energies, and spin assignments to the levels of the four high-spin bands in ^{123}Xe. Angular distribution ratios and deduced multipolarities of the transitions are listed in column 4 and 5, respectively. The initial level energies and spins of the bands have been estimated from their feeding to ND levels (see Ref. [20] and the text of this paper). W, X, Y, and Z are unknown excitation energies.

Energy E_γ (keV)	Initial level energy E_i (keV)	Spin Assignment $I_i^\pi \rightarrow I_f^\pi$	Angular distribution ratio R_θ	Multipolarity Assignment
Band L1				
1287.1(6)	W+13687	$(65/2^-) \rightarrow (61/2^-)$	1.66(17)	E2
1367(1)	W+15054	$(69/2^-) \rightarrow (65/2^-)$	1.36(14)	E2
1441.5(6)	W+16496	$(73/2^-) \rightarrow (69/2^-)$	1.45(16)	E2
1518.4(6)	W+18014	$(77/2^-) \rightarrow (73/2^-)$	1.52(17)	E2
1603.0(8)	W+19617	$(81/2^-) \rightarrow (77/2^-)$	1.40(17)	E2

Energy E_γ (keV)	Initial level energy E_i (keV)	Spin Assignment $I_i^\pi \rightarrow I_f^\pi$	Angular distribution ratio R_θ	Multipolarity Assignment
1696(1)	W+21313	$(85/2^-) \rightarrow (81/2^-)$	1.42(18)	E2
1795(1)	W+23108	$(89/2^-) \rightarrow (85/2^-)$		(E2)
1898(1)	W+25006	$(93/2^-) \rightarrow (89/2^-)$		(E2)
2002(1)	W+27008	$(97/2^-) \rightarrow (93/2^-)$		(E2)
2097(2)	W+29105	$(101/2^-) \rightarrow (97/2^-)$		(E2)
2222(2)	W+31327	$(105/2^-) \rightarrow (101/2^-)$		(E2)
2304(3)	W+33631	$(109/2^-) \rightarrow (105/2^-)$		(E2)
Band L1a				
1294(1)	W+13687	$(65/2^-) \rightarrow (61/2^-)$		(E2)
1366(1)	W+12393	$(61/2^-) \rightarrow (57/2^-)$		(E2)
Band L1b				
1193(1)	W+11192	$(57/2^-) \rightarrow (53/2^-)$		(E2)
1208(1)	W+12400	$(61/2^-) \rightarrow (57/2^-)$		(E2)
1286(1)	W+12400	$(61/2^-) \rightarrow (57/2^-)$		(E2)
Band L1c				
2054(2)	W+31159	$(105/2^-) \rightarrow (101/2^-)$		(E2)
2119(3)	W+33278	$(109/2^-) \rightarrow (105/2^-)$		(E2)
Band L2				
1349(1)	X+14649	$(67/2^-) \rightarrow (63/2^-)$		(E2)
1450(2)	X+16099	$(71/2^-) \rightarrow (67/2^-)$		(E2)
1556(2)	X+17655	$(75/2^-) \rightarrow (71/2^-)$		(E2)
1660(2)	X+19315	$(79/2^-) \rightarrow (75/2^-)$		(E2)
1762(2)	X+21077	$(83/2^-) \rightarrow (79/2^-)$		(E2)
1830(3)	X+22907	$(87/2^-) \rightarrow (83/2^-)$		(E2)
1854(3)	X+24761	$(91/2^-) \rightarrow (87/2^-)$		(E2)
1941(3)	X+26702	$(95/2^-) \rightarrow (91/2^-)$		(E2)
Band L3				
1390(1)	Y+15140	$(69/2^-) \rightarrow (65/2^-)$		(E2)
1440(1)	Y+15140	$(69/2^-) \rightarrow (65/2^-)$		(E2)
1493(1)	Y+16633	$(73/2^-) \rightarrow (69/2^-)$		(E2)
1574(1)	Y+18207	$(77/2^-) \rightarrow (73/2^-)$		(E2)
1662(1)	Y+19869	$(81/2^-) \rightarrow (77/2^-)$		(E2)
1758(1)	Y+21627	$(85/2^-) \rightarrow (81/2^-)$		(E2)
1858(1)	Y+23485	$(89/2^-) \rightarrow (85/2^-)$		(E2)
1958(2)	Y+25443	$(93/2^-) \rightarrow (89/2^-)$		(E2)
2063(2)	Y+27506	$(97/2^-) \rightarrow (93/2^-)$		(E2)
2159(2)	Y+29665	$(101/2^-) \rightarrow (97/2^-)$		(E2)
2257(3)	Y+31922	$(105/2^-) \rightarrow (101/2^-)$		(E2)
Band L3a				
1372(1)	Y+10718	$(57/2^-) \rightarrow (53/2^-)$		(E2)
1458(1)	Y+13700	$(65/2^-) \rightarrow (61/2^-)$		(E2)
1524(1)	Y+12242	$(61/2^-) \rightarrow (57/2^-)$		(E2)
Band L4				
1354(1)	Z+13354	$(65/2^+) \rightarrow (61/2^+)$		(E2)
1418(1)	Z+14772	$(69/2^+) \rightarrow (65/2^+)$	1.70(20)	E2
1517(1)	Z+16289	$(73/2^+) \rightarrow (69/2^+)$		(E2)
1612(1)	Z+17901	$(77/2^+) \rightarrow (73/2^+)$		(E2)
1709(1)	Z+19610	$(81/2^+) \rightarrow (77/2^+)$		(E2)
1803(1)	Z+21413	$(85/2^+) \rightarrow (81/2^+)$		(E2)
1886(1)	Z+23299	$(89/2^+) \rightarrow (85/2^+)$		(E2)

Energy E_γ (keV)	Initial level energy E_i (keV)	Spin Assignment $I_i^\pi \rightarrow I_f^\pi$	Angular distribution ratio R_θ	Multipolarity Assignment
1964(2)	Z+25263	$(93/2^+) \rightarrow (89/2^+)$		(E2)
2013(3)	Z+27276	$(97/2^+) \rightarrow (93/2^+)$		(E2)
2065(2)	Z+29341	$(101/2^+) \rightarrow (97/2^+)$		(E2)
2152(2)	Z+31493	$(105/2^+) \rightarrow (101/2^+)$		(E2)
2190(3)	Z+33683	$(109/2^+) \rightarrow (105/2^+)$		(E2)
Band L4a				
(936)(1)	Z+5576	$(41/2^+) \rightarrow (37/2^+)$		(E2)
(1079)(1)	Z+6655	$(45/2^+) \rightarrow (41/2^+)$		(E2)
1189(1)	Z+12000	$(61/2^+) \rightarrow (57/2^+)$		(E2)
1218(1)	Z+7873	$(49/2^+) \rightarrow (45/2^+)$	1.45(16)	E2
1270(1)	Z+10657	$(57/2^+) \rightarrow (53/2^+)$		(E2)
1294(1)	Z+12000	$(61/2^+) \rightarrow (57/2^+)$		(E2)
1343(1)	Z+12000	$(61/2^+) \rightarrow (57/2^+)$		
1351(1)	Z+9224	$(53/2^+) \rightarrow (49/2^+)$		(E2)
1354(1)	Z+12000	$(61/2^+) \rightarrow (57/2^+)$		(E2)
1433(1)	Z+10657	$(57/2^+) \rightarrow (53/2^+)$		(E2)
1483(1)	Z+10706	$(57/2^+) \rightarrow (53/2^+)$		(E2)

III. RESULTS AND LEVEL SCHEME

The investigation of the low- and medium-spin states in ^{123}Xe was based on the data set also used recently in Ref. [20]. In the present article, we report the observation of four new highly-deformed bands in this nucleus. The partial level scheme of ^{123}Xe including the new high-spin bands (L1-L4) is displayed in Fig. 1. Some of the low- and medium-spin sequences, receiving decays from the high-spin bands, are included in Fig. 1. The nomenclature of the ND bands has been adopted from the previous work [20].

Band L1 is the most intense and collects approximately 1.5% of the intensity observed for the 617-keV transition of band 9. The second-most intense band is L4, with $\approx$ 1% intensity followed by bands L3 and L2, having intensities of less than 1% each. Due to their low intensities and the possible fragmentation of their decay patterns, linking transitions to the ND levels could not be established uniquely. Spin and parity quantum numbers for states in these bands have therefore been estimated from their feeding to ND levels. In this estimate, one or two missing transitions of dipole/quadrupole nature have been assumed. The transition energies, tentative spins and excitation energies of the bands are summarized in Table I. Angular distribution ratios, R_θ, used for determining multipolarities were measured for some of the transitions of bands L1 and L4 and these are also listed in Table I. The ratios are consistent with the E2 character of the γ rays. For other transitions of the bands, the ratio could not be determined due to insufficient statistics and a quadrupole multipolarity has been assumed based on the distinct rotational character of the sequences. With the tentative spins assigned to the bands, they extend to spin $I \approx 60$. The highest spins are comparable with those assigned to the high-spin bands in neighboring Xe nuclei [17–19].

The level scheme has been constructed using $\gamma - \gamma$ coincidence relationships. Quadruple-coincidence conditions have been used to avoid possible contamination from other nuclei populated in this reaction. The in-band transitions have been placed according to their relative intensities. For very weak transitions, e.g. transitions at the top and bottom of the bands, it was difficult to verify coincidence relationships using direct coincidence gates placed on the γ rays involved. These transitions were only observed in summed spectra using gates on a list of other γ rays in the bands. The γ-ray spectra of the four newly established high-spin bands are displayed in Figs. 2, 3, and 4.

In the present work, the transitions linking the high-spin bands to levels of ND bands could not be established due to fragmentation of their decay. Excitation energies and spin values assigned to the new bands were estimated from their feeding pattern to the highest observed levels of the ND bands in the coincidence spectra. In this decay, one or two missing transitions of dipole or quadrupole character and with energies close to those near the botom of the high-spin bands have been assumed. Thus, the spins adopted in Fig. 1 have to be considered as lower limits. Furthermore, the relative intensities of the bands have been included in the estimate of the excitation energies.

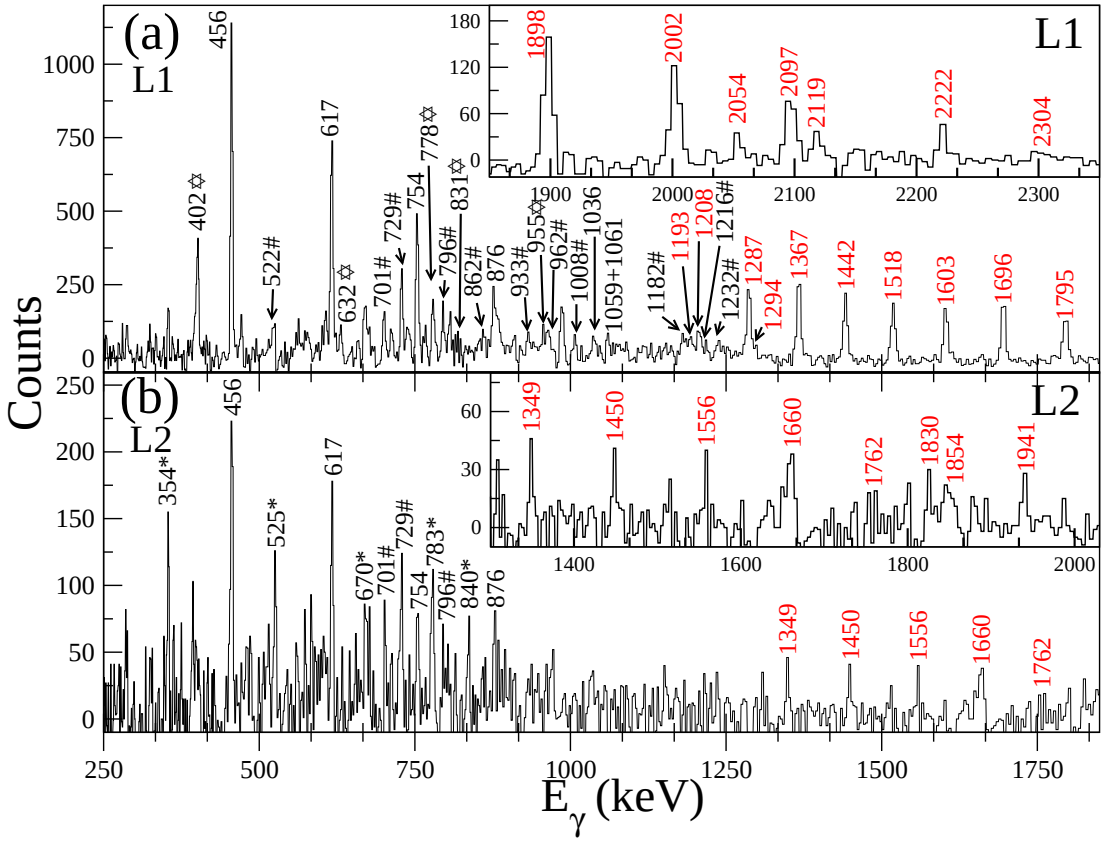

FIG. 2: (Color online) Background-subtracted summed triple-gated γ-ray coincidence spectra of bands L1 and L2 in ^{123}Xe. The gate list in (a) consists of 1287, 1367, 1442, 1518, 1603, 1696, 1795, 1898, and 2002 keV transitions of band L1 and the list in (b) includes 1349, 1450, 1556, 1660, 1762, 1830, 1854, and 1941 keV γ energies from band L2. The #-marked peaks in (a) denote γ rays from bands 1 and 2 to which band L1 decays. The star-marked peaks in (a) are γ rays of bands 7 and 8. The peaks marked by asterisks in (b) are γ rays of ^{124}Xe and are appearing in the spectrum due to overlapping energies in the coincidence gates. The insets in both spectra show the higher-energy in-band transitions of the respective bands.

A. Band L1

Band L1, consisting of a cascade of twelve γ rays, is the most intense sequence above $I = 30$ in this nucleus. A summed triple-gated coincidence spectrum with gates on the transitions of band L1 is presented in Fig. 2(a). The decay of L1 is fragmented and the total intensity of the band is divided among several cascades feeding to bands 1, 2, 6, 7, 8, and 9, respectively. This is observed in Fig. 2 (a), where the intensities of the transitions below the 1287-keV γ ray drop drastically. Parallel branches, labeled L1a and L1b, have been detected in the lower part of this structure. The 1294-keV transition is missing in the 1287-keV coincidence spectrum and has been placed in parallel to it. The presence of the 1366- and 1286-keV γ rays has been established in coincidence spectra with respective gates on the 1367- and 1287-keV transitions of the band. The 1366-keV transition was not observed in gates involving both the 1367- and 1287-keV transitions and, therefore, it is placed in parallel to the 1287-keV γ rays. The band L1 also forks into two branches at high spin, where the parallel branch is labeled L1c.

In a triple-gated coincidence spectrum, produced with a list of all the transitions of band L1 (see Fig. 2 (a)), the transitions of band 1 up to the 1232-keV transition and of band 2 up to the 1216-keV transition along with some of the intermediate M1 γ rays have been observed. A fraction of the band intensity is feeding the $55/2^-$ state of band 9 and the $59/2^-$ level of band 7. In a triple-gated spectrum with two transitions of band L1 and the third one of 402 keV of band 6, all the transitions of band L1 along with those of 955, 632, and 831 keV of bands 7 and 8 were observed. Furthermore, the 955-keV transition is present in a triple-gated spectrum with a gate on the 1287 line and two gates on the rest of the transitions of band L1 but the 632 and 831 keV γ rays are absent. This indicates that the 1287 keV transition is feeding the $59/2^-$ level of band 7. Assuming a missing linking transition of dipole nature and energy around 1300 keV, a tentative spin of $61/2^-$ and an excitation energy of about 12.4 MeV can be assigned to the lowest level of band L1. With a possibility that the missing transition is of quadrupole character or that an additional linking

γ ray is present, the uncertainty in the spin assignment is 1-3 $\hbar$ and that for excitation energy about 1-2 MeV.

B. Band L2

Band L2 is the least intense of the four high-spin bands and it is difficult to conclude exactly where this band is feeding to ND levels. Only the strongest transitions of the yrast band 9 are visible in a triple-gated spectrum produced with a list of γ rays of band L2 (see Fig. 2 (b)). The strongest γ rays of ^{124}Xe are also visible due to overlapping energies with some of the transitions of the L2 band. The spin and excitation energy of the band have been adjusted to place this sequence above all other bands observed in this nucleus. A tentative spin of 63/2 and an energy around 13.3 MeV are being proposed for the band head in the level scheme (see Fig. 1).

C. Band L3

Band L3 exhibits regular energy spacings above the 1493-keV transition with nearly 100 keV energy difference between successive γ rays. The energy difference becomes irregular in its extension toward lower energy, marked as L3a. The ordering of γ rays below the 1493-keV transition is based on their intensities in different coincidence spectra. However, a possible reordering cannot be ruled out due to their weak intensities. A 1390-keV γ ray, forming a parallel decay branch is observed at the bottom of the band.

Band L3 decays primarily to band 9 but it also feeds bands 6 and 7. A summed triple-gated coincidence spectrum with gates on all the transitions of the band is displayed in Fig 3 (a). The strongest γ rays of band 9 and the 402, 778, and 955-keV transitions of band 7 are clearly visible. A triple-gated spectrum with two gates placed on a list of transitions of band L3 and the third gate on the 402-keV transition of band 7 confirms the presence of the 778, 955, and 1402-keV γ rays of band 7 along with all those of band L3 (see Fig. 3 (b)). A very small peak at 1440 keV, the transition placed below the 1493 keV one in L3, is also visible in that spectrum. Furthermore, a summed triple-gated spectrum with gates on 402- and 1402-keV γ rays and on one transition from band L3 confirms the presence of the 1440-keV line of L3. Therefore, assuming a missing dipole transition of 1200 keV, a spin 65/2 and 13.7 MeV of excitation energy is proposed to the lowest level of band L3.

D. Band L4

Among the high-spin bands, L4 has the longest chain of in-band transitions.The band is regular in energy at the beginning with successive γ-ray energy differences of the order of 100 keV. The difference gradually decreases to 80 keV towards higher spin. The γ-ray energies become irregular at higher spin indicating the presence of a band crossing. The top two transitions of the band, i.e. the 2152- and 2190-keV γ rays, were observed only in summed triple-gated spectra produced using a list of the other transitions of the band. Due to low statistics in the resulting spectra a unique placement of the 2152- and 2190-keV transitions was not possible. The most probable placement is that they are extensions of band L4 on top of the 2065-keV line, although a placement in parallel to that transition cannot be excluded.

Band L4 predominantly decays to bands 12 and 13. A summed triple-gated coincidence spectrum, created with a list of transitions of band L4, is found in Fig. 4 (a). The transitions of bands 12 and 13 can be seen in coincidence with the transitions of the sequence. A triple-gated spectrum with two gates on transitions of L4 and the third gate on the 180-keV transition of bands 12 and 13 also shows γ rays of band L4 along with transitions of bands 12 and 13. Similar to other high-spin bands in this nucleus, the decay of L4 is also fragmented and several decay branches below the 1354-keV transition have been observed in the coincidence analysis. The presence of a second 1354-keV γ ray is shown in the inset of Fig.4 (a). A decay branch of 1294- and 1483-keV γ rays has been observed in parallel to the 1343- and 1433-keV transitions. The transitions below the 1433-keV γ ray of L4a were not only in coincidence with the band transitions but also with themselves. Due to overlapping energies of some of the γ rays, e.g. the 1343-, 1351-, and 1354-keV lines and the 1079- and 1080- decay transitions of bands 12 and 13, clean gates could not be placed on individual transitions. Therefore, the ordering of the transitions in the lower part of the band remains uncertain.

In order to estimate the spin of the band, feedings from band L4 to bands 12 and 13 have been searched for in the coincidence spectra. It is observed in Fig. 4 (a) that the transitions from higher-spin states of bands 12 and 13, e.g. the 463-, 670-, and 965-keV lines, are present along with other intense transitions of the bands. The presence of the 944-keV transition in the spectrum is not clear. Therefore, band L4 most likely feeds band 12 and 13 in the spin 53/2-55/2 region. The 1189-, 1270-, and 1354-keV transitions at the bottom of the band are possible decay-out branches from L4. Considering two missing transitions of quadrupole nature feeding on top of the $53/2^+$ state of band 12, a spin 61/2 can be tentatively proposed to the level below the 1354 keV transition. If the average energy of these two transitions is 1300 keV, an excitation energy of roughly 12.0 MeV can be esti-

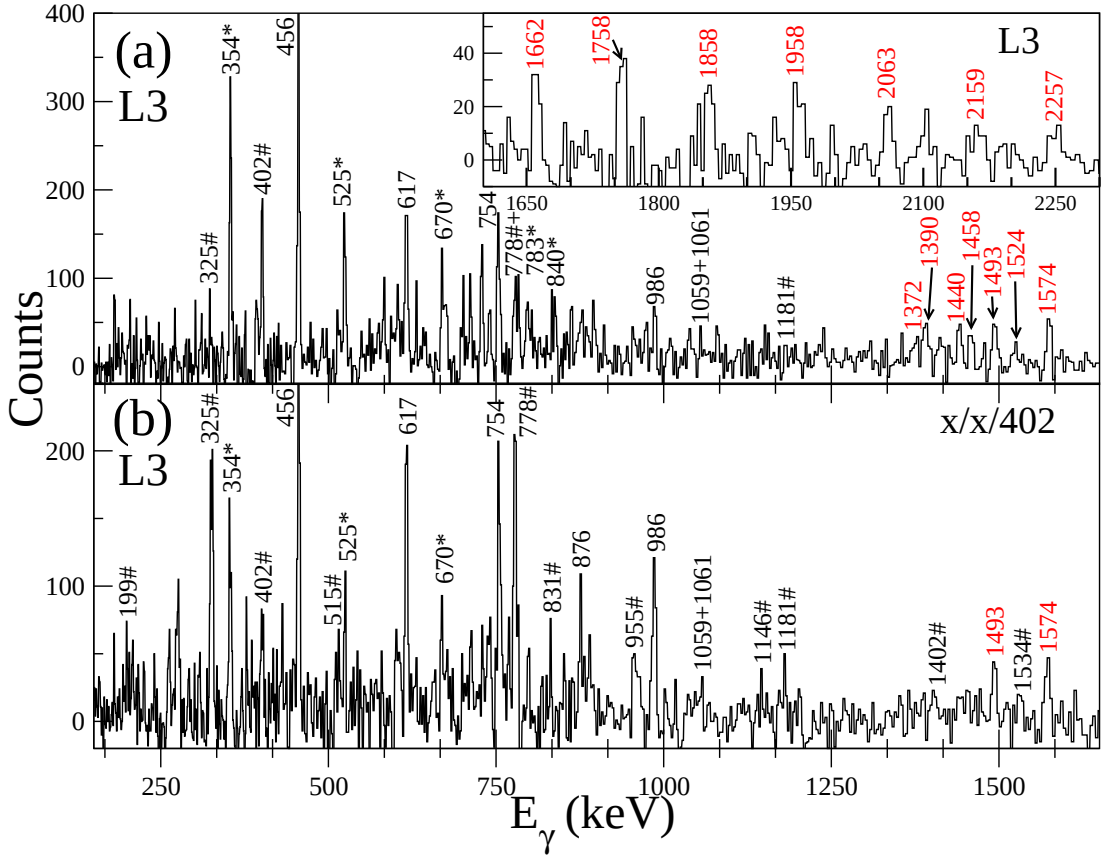

FIG. 3: (Color online) Background-subtracted summed triple-gated γ-ray coincidence spectra representative of band L3 in ^{123}Xe. In panel (a), triple gates have been placed on a list 'x' consisting of 1493-, 1574-, 1662-, 1758-, 1858-, 1958-, 2063-, and 2159-keV transitions of band L3. The inset in (a) shows the higher-energy in-band transitions of band L3. In (b), the spectrum has been generated with two gates on the list 'x' in (a) and the third gate on the 402-keV transition of bands 7 and 8. The peaks marked by a # symbol represent γ rays from bands 6-8. The contaminant peaks of ^{124}Xe are marked by asterisks.

mated to the level. Assuming a quadrupole nature of the transitions of band L4a, the lowest level of the band can be proposed to have spin 37/2 at an excitation energy of about 4.64 MeV. With these assumptions for spin and excitation energy, the lower portion of L4a is lower in energy by nearly 0.8 MeV relative to bands 12 and 13. The parity of the band has been assumed to be positive.

IV. DISCUSSION

In this section, the observed bands will be compared with the lowest-energy bands calculated within the cranked Nilsson-Strutinsky (CNS) [23–25] and cranked Nilsson-Strutinsky-Bogoliubov (CNSB) [26, 27] formalisms. The tentative spins and parities assigned to the bands in Fig. 1 will be compared with those suggested from the theoretical analysis. A brief discussion on the impact of the pairing interaction in the calculated bands will be made by comparing results of the CNS and CNSB models.

A. The CNS and CNSB models

Within the CNS formalism, the Hamiltonian has the form [23–25]

$$H = H_{MO}(\varepsilon_2, \gamma, \varepsilon_4) - \omega j_x, \qquad (1)$$

where H_{MO} is the modified oscillator Hamiltonian [28] and ωj_x is the cranking term for rotation around the principal x axis. The κ and μ parameters derived for the $A \approx 110$ region have been applied [24]. The total energy is defined as the sum of the shell energy and the rotating liquid drop energy. This shell energy is calculated using the Strutinsky method [29, 30]. The Lublin-Strasbourg drop (LSD) model [31] is used for the static liquid drop energy with the rigid-body moment of inertia calculated with a radius parameter $r_0 = 1.16$ fm and diffuseness parameter $a = 0.6$ fm [25].

The total energy is minimized with respect to the deformation parameters $(\varepsilon_2, \varepsilon_4, \gamma)$ for each configuration and for for each spin value. Special methods, based on exact and approximate quantum numbers, are introduced

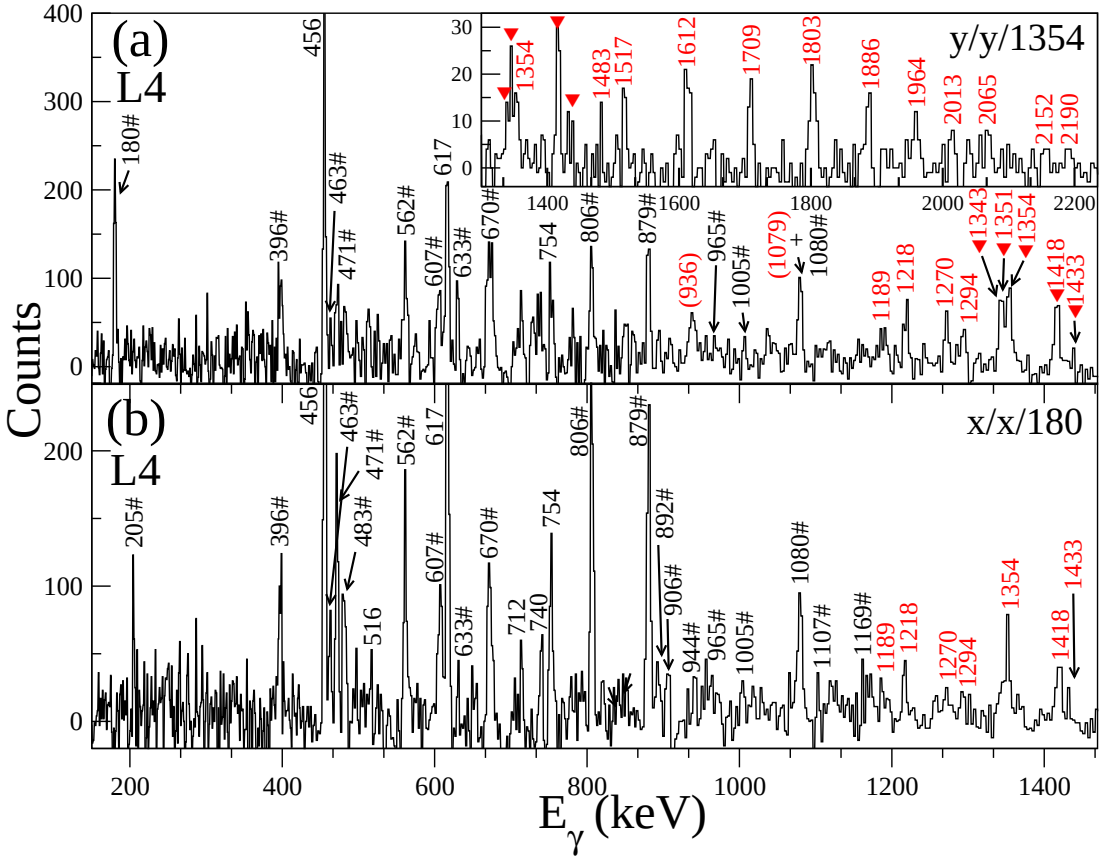

FIG. 4: (Color online) Background-subtracted summed triple-gated γ-ray coincidence spectra for band L4 in ^{123}Xe. In panel (a), triple gates have been placed on a list, 'x', consisting of 1354-, 1418-, 1517-, 1612-, 1709-, 1803-, 1886-, and 1964-keV γ rays of band L4. In the inset of panel (a), triple gates with two gates on the list, 'y' of 1418-, 1517-, 1612-, 1709-, 1803-, 1886-, 1964-, and 2013-keV transitions of L4 and the third gate on 1354- keV γ ray. The second 1354-keV (and 1351-keV) energy peak can be seen. The panel (b) presents a triple-gated summed spectrum with two gates on list 'x' defined in (a) and the third gate is on the 180-keV transition of bands 12 and 13. The peaks marked by # represent γ rays from bands 12 and 13 (see Ref. [20] for detail level scheme) to which band L4 decays.

[23, 32] to fix diabatic configurations in a detailed way. These calculated configurations are labeled as

$$[(p_1)p_2p_3; n_1n_2(n_3n_4)]$$

relative to a $Z = 50$ and $N = 70$ core, where p_1 is the number of proton holes in orbitals of $g_{9/2}$ character, p_2 the number of dg protons (i.e. protons with dominant amplitudes in the $d_{5/2}$ and $g_{7/2}$ shells) and p_3 the number of protons in $h_{11/2}$ orbitals. Furthermore, n_1 is the number of $\mathcal{N} = 4$ neutron holes, n_2 the number of $h_{11/2}$ neutrons, and n_3 and n_4 are the numbers of fh and $i_{13/2}$ neutrons, respectively, where fh refers to orbitals with their main amplitude in the $f_{7/2}$ and $h_{9/2}$ shells. Numbers in parenthesis are not shown when they are equal to zero. When appropriate, the signature for an odd number of particles in a certain group is denoted by a subscript, + or −. In previous publications, when signature was not specified, a shorter form $[p_1p_3, n_2(n_3n_4)]$ was used to label the configuration, e.g. see refs. [15–17]. It is generally assumed that each of the labels, p_1, p_2, etc. has only one digit. In the event that a label has two digits, e.g. 10 holes in the $\mathcal{N} = 4$ neutron shell, a '$_*$' is added as a subscript.

In the CNSB formalism [26, 27], the same potential as in the CNS one plus a monopole pairing term, is used

$$H = H_{MO}(\varepsilon_2, \gamma, \varepsilon_4) - \omega j_x + \Delta(P^\dagger + P) - \lambda\hat{N}, \quad (2)$$

where $P^\dagger$ (P) and $\hat{N}$ are the pair creation (annihilation) and particle number operators, respectively. The formalism is based on the ultimate cranker method developed by T. Bengtsson [33]. In the CNSB formalism, the microscopic energy, after particle number projection, is minimized not only in the deformation space, but also in a mesh of the pairing parameters, Fermi energies λ_p and λ_n, and pairing gaps Δ_p and Δ_n. According to the Hamiltonians in eqs (1) and (2), the only difference between the CNS and the CNSB yrast configurations is the pairing energy. In the CNSB formalism, the only preserved quantum numbers are parity π and signature α for protons and neutrons. Thus, it is possible to form 16 different configurations which can be labeled $(\pi, \alpha)_p(\pi, \alpha)_n$.

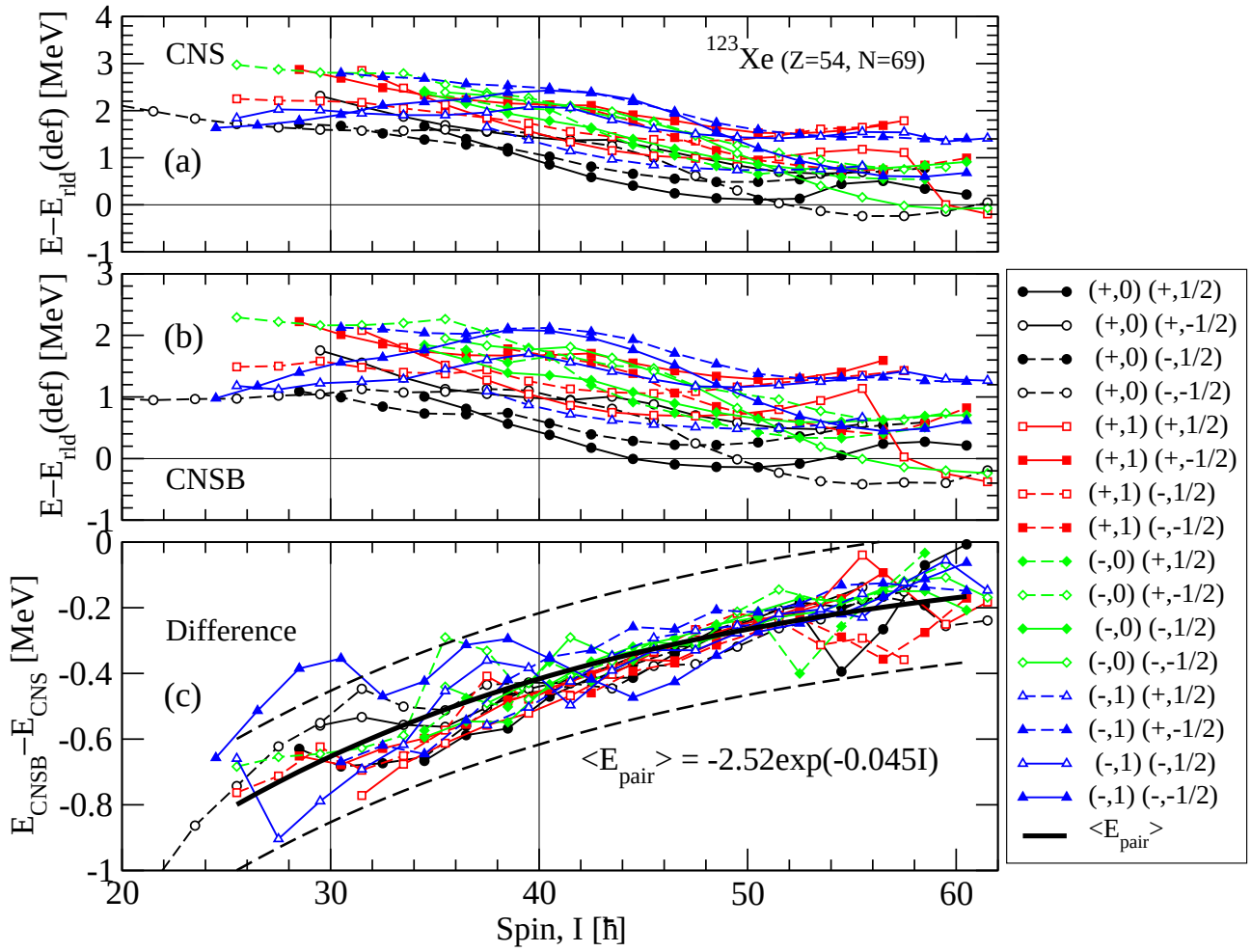

FIG. 5: (Color online) The energy of the minimum at $\varepsilon_2 \approx 0.3$ and a small γ deformation is shown relative to the rotating liquid drop model as calculated in the CNS model (a) and the CNSB model (b) for the 16 configurations with fixed parity and signature for protons and neutrons. The difference between these two calculations is presented in panel (c) where it is fitted to an exponential function labelled $< \mathrm{E_{pair}} >$. Note the expanded scale in the lower panel, where dashed lines illustrate the fact that almost all differences are fitted with an accuracy better than ± 0.2 MeV.

B. The pairing energy

As discussed in Ref. [17], the configurations with two holes in the $g_{9/2}$ shell are favored in energy and one should consider those to find an interpretation for the high-spin collective bands in the Xe region. Such configurations form minima for $I \approx 30-60$ at $\varepsilon_2 \approx 0.30 \pm 0.05$ and $\gamma \approx 0 \pm 15°$. If the energy of these minima is calculated in the CNS and CNSB formalisms, i.e. with and without pairing, see Fig. 5, it turns out that the pairing energy is always small and, moreover, that it follows a smooth trend with spin. Thus, for $I > 30$ and for all 16 combinations of parity and signature for protons and neutrons, $(\pi,\alpha)_p(\pi,\alpha)_n$, Fig. 5 indicates that the pairing energy is generally smaller than 0.7 MeV and it comes close to zero when the spin approaches $I = 60$. Especially, it can be fitted with an exponential function,

$$\langle E_{pair} \rangle = -2.52 \cdot \exp\left(-0.045 I\right)$$

, where, with very few exceptions, the values are approximated within ± 0.2 MeV. Thus, when the unpaired energy is complemented with an average pairing energy, these calculated energies lie close to the energies with the proper pairing energy. However, by considering the unpaired configurations, it becomes possible to trace these in a detailed way. This also allows to consider configurations which are not yrast within the paired configurations $(\pi,\alpha)_p(\pi,\alpha)_n$. We will refer to these calculations within the CNS formalism but with addition of an average pairing, as the CNS(B) formalism.

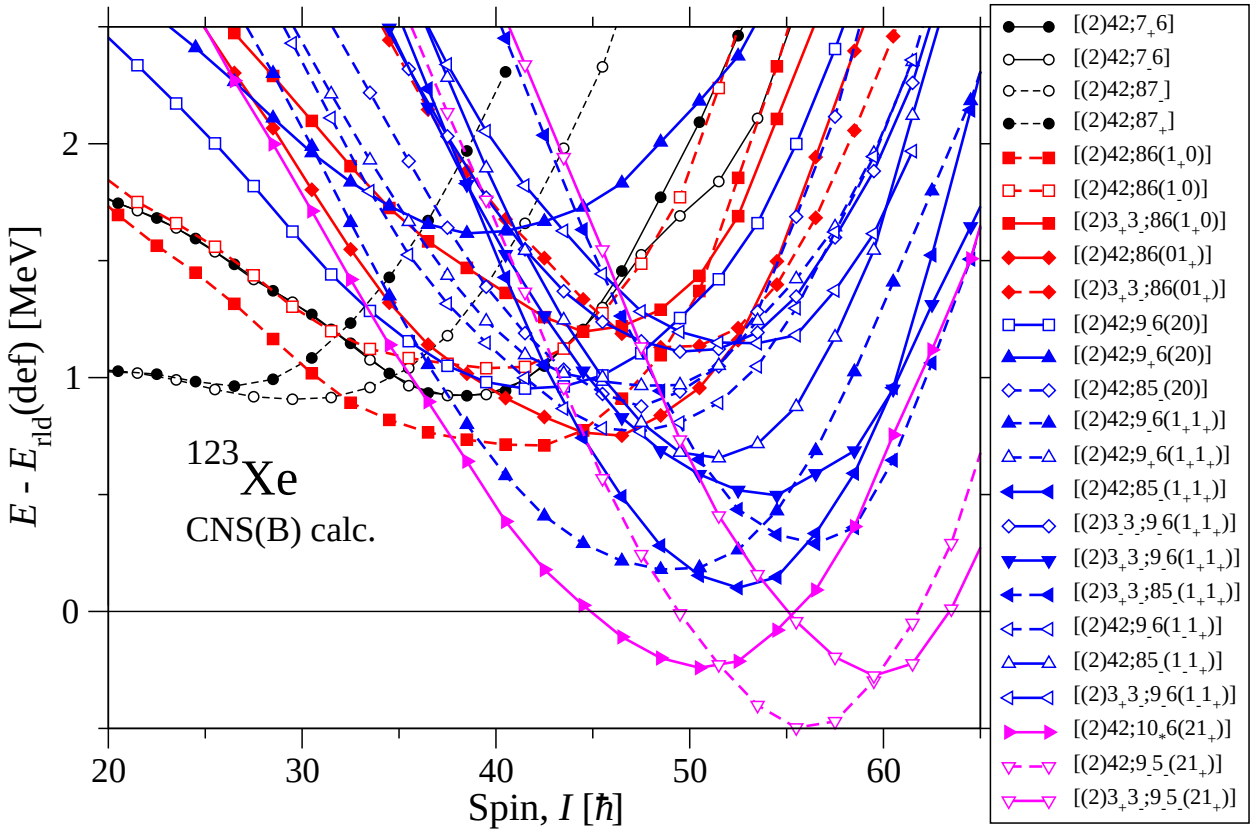

FIG. 6: (Color online) The energy of the lowest-lying configurations with two $g_{9/2}$ proton holes calculated in the CNS model with the average pairing energy added, CNS(B), are shown relative to the rotating liquid drop energy. Different colors are used depending on the number of neutrons excited across the $N = 82$ gap.

C. General features when comparing observed and calculated bands

As suggested from the single-particle diagram for neutrons, the low-lying configurations have up to three neutrons excited across the $N = 82$ gap (see Fig. 12 in Ref. [17]). A large number of such configurations combined with proton configurations with two $g_{9/2}$ holes have been calculated in the CNS formalism and those which are relatively low-lying in energy have been selected. With the average pairing energy added, these configurations are displayed relative to the rotating liquid drop energy in Fig. 6. The configurations with four excited neutrons across the $N = 82$ shell gap appear to be favored in energy at much higher spin and are not of interest for the interpretation of the high-spin bands.

The excitation energies of the high-spin bands in ^{123}Xe, shown in Fig. 1 as L1-L4, have been plotted relative to the rotating liquid drop energy as a function of spin in Fig. 7. Note that the bands are not linked and their spins and excitation energies represent lower limits which have been proposed assuming that one or two missing transitions feed the levels of the ND bands. The relative energies of selected ND bands have been included in Fig. 7 for reference. The general features of the high-spin

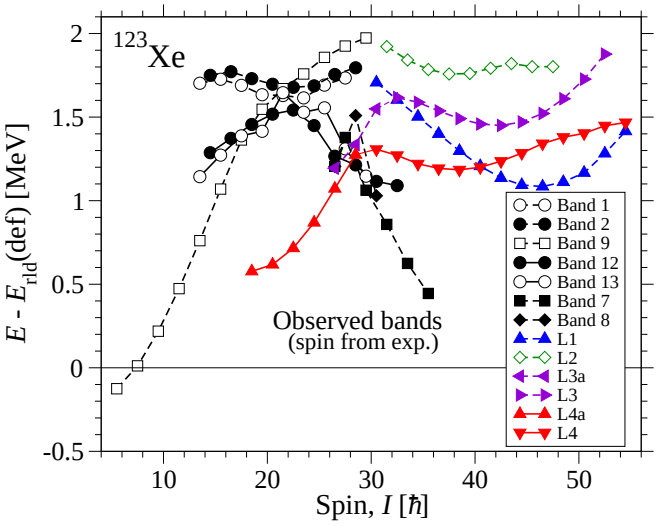

FIG. 7: (Color online) The observed collective bands in ^{123}Xe, with spin and excitation energies according to the experimental analysis, are drawn relative to the rotating liquid drop reference. In addition, some selected ND bands [20] are shown relative to the same reference.

bands are similar to those of the calculated ones in Fig. 6, i.e. smooth curves with a minimum for $I = 35 - 45$. This is especially true for bands L1 and L3 while bands L2 and L4 are more irregular suggesting that they might be built from two or three interacting bands. Furthermore, for the calculated bands which are most favored in energy, the minimum is located at a higher spin values, $I \approx 50$. This suggests that the spin values of the observed bands might be larger than the experimental values suggested in Figs. 1 and 7. This is not unexpected considering that the experimental values are lower limits.

An interesting feature of the observed bands is the sections at low spin forming short sequences, especially band L4a with five transitions and band L3a with two transitions. The fact that these bands are not linked to the ND bands suggests that they are not associated with excitations in the valence space. Thus, like the high-spin bands, it is assumed that they are built from configurations with two protons holes in the $g_{9/2}$ orbitals. As evident from Fig. 6, there are only a few low-lying configurations of this type for spin values $I \approx 30$ or below. These configurations have two protons in $h_{11/2}$ orbitals and no excitation of neutrons across the $N = 82$ shell closure. The configurations with three protons in the $h_{11/2}$ shell are located at higher energy. A comparison between experiment and calculations suggests that the spin values of band L4 should be increased so that the L4a branch becomes flat when drawn relative to the rotating liquid drop energy, see the discussion below. Then the branch L4a can be assigned to a $[(2)42; 87]$ configuration which is somewhat similar to the smooth terminating bands in the $A = 110$ region [24, 32]. In this configuration, it is rather straightforward to distinguish between dg and sd neutrons, i.e. neutrons which have their dominating amplitudes in the $d_{5/2}$, $g_{7/2}$ shells and in the $s_{1/2}$, $d_{3/2}$ shells, respectively. With such a distinction, the $[(2)42; 87]$ configuration can be written relative to a ^{114}Sn core as

$$\pi[(g_{9/2})^{-2}_{8}(dg)^{4}_{10}(h_{11/2})^{2}_{10}]_{28}\otimes$$
$$\nu[(dg)^{-4}_{10}(sd)^{2}_{2}(h_{11/2})^{7}_{16.5,17.5}]_{28.5,29.5}$$

where the maximum spin value is denoted as a subscript. Adding these spin contributions, a highest value for the total spin can be calculated, $I_{max} = 56.5,\ 57.5$. Thus, these configurations will terminate at relatively very high spin values where they are high above yrast line and probably cannot be observed as discrete states.

In Fig. 6, there are two configurations which are particularly low in energy in an extended spin range $I \approx 35-50$, namely $[(2)42; 10_{*}6(21_{+})]$ and $[(2)42; 9_{-}6(1_{+}1_{+})]$. This suggests another constraint on the configuration assignment, namely that one would expect that both of these configurations could be assigned to an observed band, L1-L4.

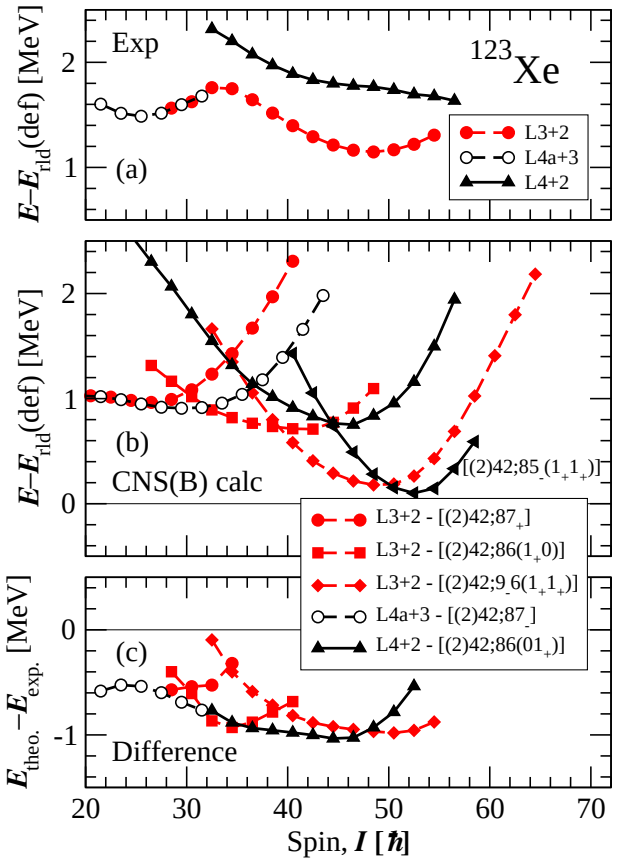

FIG. 8: (Color online) Suggested assignments for the bands L3 and L4. In the upper panel, the observed bands are drawn relative to the rotating liquid drop energy. They are labeled by the spin change which is assumed compared with the values suggested in Fig. 1. The bands calculated in the CNS(B) formalism are drawn relative to the same reference in the middle panel. The lower panel shows the difference between experiment and calculations. Note that the full L3 band including the low-spin L3a section is labeled L3. For the L4 band, it is assumed that the transition connecting L4a and L4 is of stretched $E1$ character. In the middle panel, the $[(2)42; 85_{-}(1_{+}1_{+})]$ configuration is included to show that there exists a configuration which crosses with the$[(2)42; 86(01_{+})]$ configuration at $I \approx 50$.

D. Bands L3 and L4

In order to assign configurations to the branches of L3 and L4 at lower spin, labeled as L3a and L4a in Fig. 1, these are compared in Fig. 8 to the calculated configurations which are lowest in energy in the spin range $I = 20 - 30$ of Fig. 6, i.e. the two signatures of the $[(2)42; 87]$ configuration where the occupation of the j-shells is spelled out above. It is appropriate to assign the favored signature of this configuration to the best developed low-spin band L4a where the difference curve between experiment and calculation, see Fig. 8 (c), becomes relatively constant if the spin value of band L4a is increased by 3 units compared to the values in Figs.

1 and 7. Consequently, the L3a band will have signature $\alpha = 1/2$, and if all the transitions of L3a and L3 are of stretched $E2$ character, the full spin range of the L3 band has this signature. Therefore, above the crossing, the L3 band can be assigned to the configuration, $[(2)42; 9_{-}6(1_{+}1_{+})]$, i.e

$$\pi[(g_{9/2})^{-2}(dg)^{4}(h_{11/2})^{2}]\otimes\nu[(sdg)^{-9}(h_{11/2})^{6}(hf)^{1}(i_{13/2})^{1}]$$

which is the next lowest calculated configuration for $I = 40 - 50$, see Fig. 6. With a spin value which is two units higher than that suggested suggested in Fig. 1, the energy difference for band L3 is very close to constant. Furthermore, if the energy of the bands is increased by 0.8 MeV for each added spin unit, the difference curve has essentially the same value as for the L4a band. It appears that the crossing region between the $[(2)42; 87_{+}]$ and $[(2)42; 9_{-}6(1_{+}1_{+})]$ configurations, i.e. between L3a and L3, is smoothed by the $[(2)42; 86(1_{+}0)]$, or

$$\pi[(g_{9/2})^{-2}(dg)^{4}(h_{11/2})^{2}] \otimes \nu[(sdg)^{-8}(h_{11/2})^{6}(hf)^{1}]$$

configuration. Thus, starting at low spin from the L3a band, first a neutron is excited from $h_{11/2}$ to the hf orbitals and then another neutron is lifted from $\mathcal{N} = 4$ to $\mathcal{N} = 6$.

A reasonable interpretation for band L4 becomes difficult if all the transitions are assumed of stretched $E2$ character , and parity and signature are the same throughout L4a and L4. However, if the 1343-keV transition, connecting L4a and L4, is assumed to be a $\Delta(I) = 1$, $E1$ transition, the L4 band can be assigned a configuration $[(2)42; 86(01_{+})]$ or

$$\pi[(g_{9/2})^{-2}(dg)^{4}(h_{11/2})^{2}] \otimes \nu[(sdg)^{-8}(h_{11/2})^{6}(i_{13/2})^{1}],$$

which means that an $h_{11/2}$ neutron is lifted to the $i_{13/2}$ in the transition from the L4a to the L4 band. With this assignment, the difference curve will essentially overlap with that for the L3 band, see Fig. 8. The agreement is seen up to $I \approx 48$ where a bandcrossing is apparent in the L4 band. A bandcrossing is also observed in the calculation for the $[(2)42; 85_{-}(1_{+}1_{+})]$ configuration, where the calculated crossing is much sharper than the observed one. However, because the experimental values are rather uncertain at these high spin values, this should not be viewed as a serious disagreement.

E. Bands L1 and L2

Band L1 is regular in its full spin range. If its spin values are increased by $2\hbar$ relative to the ones adopted in Fig. 1, it can be assigned to the configuration which is calculated lowest in energy for $I \approx 38 - 54$, $[(2)42; 10_{*}6(21_{+})]$ or

$$\pi[(g_{9/2})^{-2}(dg)^{4}(h_{11/2})^{2}]\otimes\nu[(sdg)^{-10}(h_{11/2})^{6}(hf)^{2}(i_{13/2})^{1}],$$

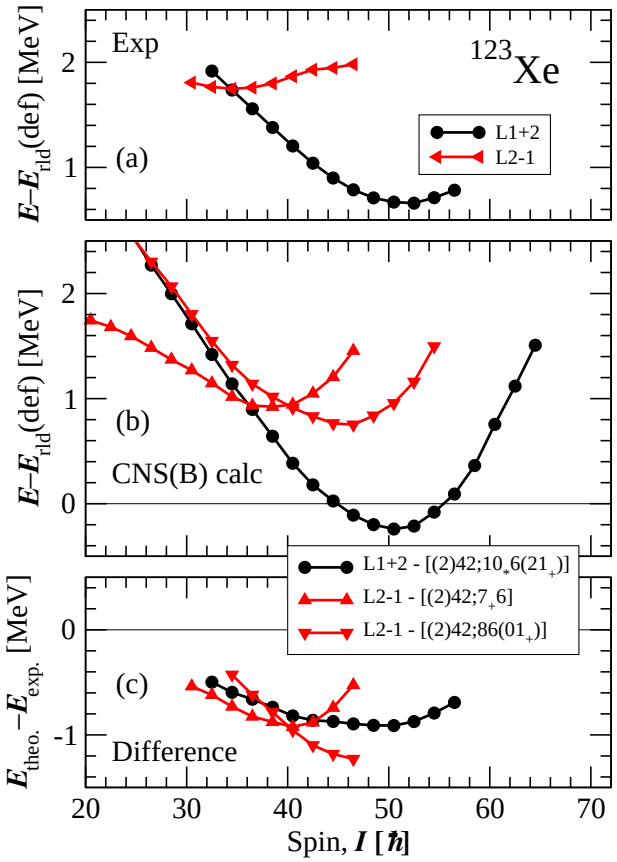

FIG. 9: (Color online) Same as Fig. 8 but for the L1 and L2 bands.

see Fig. 9. The low calculated energy of this configuration with three neutrons excited across the $N = 82$ gap and the nice agreement between experiment and calculations support this assignment.

Band L2 is much shorter and more irregular which means that any assignment will be uncertain. As shown in Fig. 9, if its spin value is decreased by $1\hbar$ relative to the value in Fig. 1, it might be assigned to the $[(2)42; 7_{+}6]$ configuration at low spin and possibly to a configuration with one neutron lifted from $\mathcal{N} = 4$ to $\mathcal{N} = 6$ at higher spins. However, the calculated crossing appears sharper than the observed one. Furthermore, the suggested configuration above the crossing was already assigned to band L4. Thus, if that assignment is correct, another interpretation for the highest spin states in the L2 band is needed. However, as the observed values for the highest spin states in the L2 band are rather uncertain, we will not try to propose an alternative interpretation.

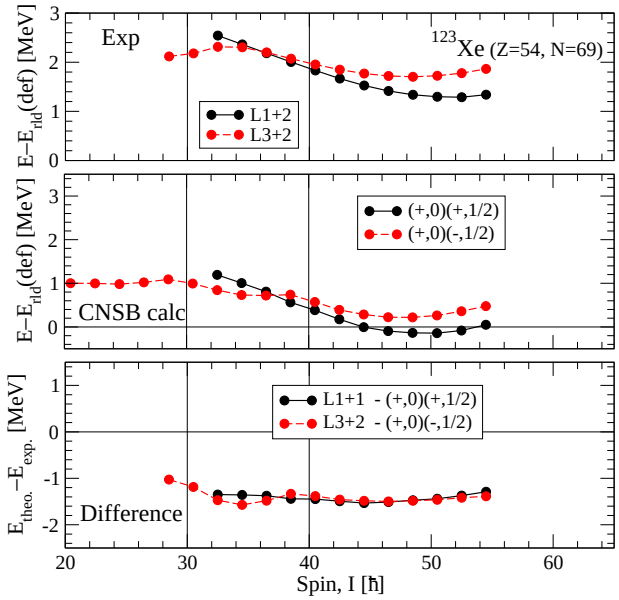

FIG. 10: (Color online) Comparisons between the observed bands L1 and L3 and the CNSB configurations assigned to them according to the comparison with CNS configurations, see Figs. 8 and 9.

F. Energies and energy surfaces in the CNSB formalism

If a configuration assigned to an observed band is the lowest one in a $(\pi,\alpha)_p(\pi,\alpha)_n$ group, it is straightforward to compare it with the full CNSB calculations. This is demonstrated for bands L1 and L3 in Fig. 10 which can be compared with the corresponding curves in Figs. 9 and 8, respectively. Considering that the full pairing can be described by the average pairing with a good accuracy, see Fig. 5, the difference between calculations and experiment will be similar to that of the CNS calculations with the average pairing energy added, i.e. the CNS(B) calculations.

The change in CNS configuration at low spin in the L3 band can be seen in the energy surface for the (+,0)(-,1/2) configuration in Fig. 11, calculated in the full CNSB formalism. For $I = 34.5$, the lowest-energy configuration is $[(2)42; 86(1_+0)]$ corresponding to the deformation $\varepsilon_2 \approx 0.28$, $\gamma \approx 3°$ while the minimum at $\varepsilon_2 \approx 0.32$, $\gamma \approx 10°$ for $I = 44.5$ is formed with a neutron excited from $\mathcal{N} = 4$ to $\mathcal{N} = 6$, i.e. in the $[(2)42; 9\_6(1_+1_+)]$ configuration. At intermediate spins, $I = 38.5,\ 40.5$, coexistent minima are calculated.

G. Summary of the assignments

The spin values and corresponding excitation energies which are suggested from the CNS calculations are summarized in Table II. In the determination of the excitation energies we started from the experimental values specified in Fig. 1 and 0.8 MeV was added for each spin unit. The values in bands L4 and L4a have been increased by 3×0.8 MeV, considering that the spin values in band L4a are increased by $3\hbar$. Note, however, that the values in the L4 band are increased by only $2\hbar$. In any case, with these energies, the difference between ex-

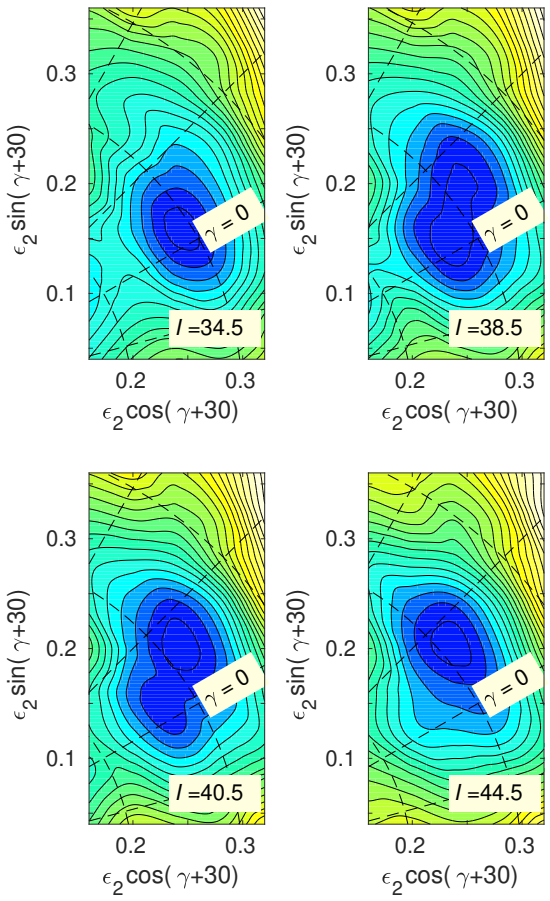

FIG. 11: (Color online) Total energy surfaces calculated in the CNSB formalism with constraints of parity and signature for protons and neutrons, $(\pi,\alpha)_p(\pi,\alpha)_n = (+,0)(-,1/2)$. This is the configuration assigned to the L3 band. The contour line separation is 0.2 MeV.

TABLE II: The spin values I_f and energy E_f which is assumed for the state which is fed by the transition $(E_\gamma)_f$ in the theoretical assignments for the different bands.

Band	$(E_\gamma)_f$ (MeV)	$I_f(\hbar)$	E_f (MeV)
L1	1.287	$65/2^-$	14.0
L2	1.349	$61/2^-$	12.5
L3a	1.349	$57/2^-$	10.946
L3	1.440	$69/2^-$	15.3
L4a	0.936	$43/2^+$	7.040
L4	1.354	$65/2^+$	14.4

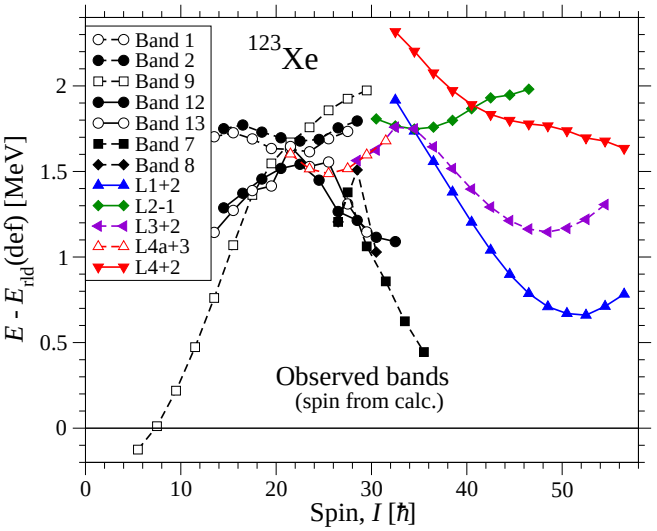

FIG. 12: (Color online) The observed collective bands in ^{123}Xe with spin values and excitation energies chosen from the comparison with calculated configurations are shown relative to the rotating liquid drop reference. In addition, some selected normal-deformed bands [20] are included.

periment and calculations has essentially the same value in all bands, see Figs. 8(c) and 9(c). Using the values in Table II, the collective bands are displayed together with selected ND bands in Fig. 12. Comparing with the calculated bands in Fig. 6, the assignments for bands L1 and L3 appears convincing, since they agree with the two configurations calculated lowest in energy for $I \approx 40-50$. The observed bands evolve smoothly with spin for at least 20 spin units and, in this spin range, the configurations assigned to them do not cross with any other ones having the same parity and signature. Furthermore, it is gratifying that the most intense band, L1, is assigned to the configuration which is calculated to be lowest in energy. However, the third most intense band, L3, is assigned to a configuration which is calculated $0.5-1.0$ MeV higher in the spin range $I = 30-50$. The relative energies are rather sensitive to parameter changes while moments of inertia that reflect the overall features of the $E - E_{rld}$ plots are much more stable towards changes in parameters.

For the assignment of bands L4 and L4a, it would be important to measure the multipolarity of the 1343-keV transition connecting these two bands. Band L1 is mainly feeding negative-parity states which might suggests that it has negative parity contrary to the assignment of a positive-parity configuration. However, it is not unlikely that the band is linked through an $E1$ transition. For the other bands where the feeding can be analyzed, L3 and L4, the suggested parity appears in line with the assumption that it is not changed by the connecting transitions.

V. SUMMARY

High-spin states in ^{123}Xe were populated in a heavy-ion induced fusion-evaporation reaction and $\gamma-\gamma$ coincidence relationship were measured with the Gammasphere spectrometer. Four new highly-deformed rotational bands have been observed up to high spins which feed previously known levels of ND bands [20] around spin $I \approx 30$. However, linking transitions between the high-spin bands and the levels of known spin and parity could not be established. Excitation energies and spin values of the bands are estimated on the basis of their feeding to ND levels under the assumption of a deexcitation through one or two unobserved γ-ray transitions.

The properties of the bands are compared with those calculated within the CNS and CNSB formalisms, where the method with an average pairing added to the CNS energies, CNS(B) appears to be particularly useful. The calculations indicate that the bands correspond to deformed minima around $\varepsilon_2 \approx 0.3$ and $\gamma \approx 5°$ which are formed by excitation of two protons from the $g_{9/2}$ orbitals across the $Z = 50$ shell gap along with neutron excitations across the $N = 82$ gap to the fh ($f_{7/2}h_{9/2}$) and $i_{13/2}$ orbitals. Indeed, all the observed bands are assigned to the proton configuration labeled '(2)42', i.e. with four particles in dg ($d_{5/2}g_{7/2}$) orbitals and two in $h_{11/2}$ orbitals.

In order to find a satisfactory agreement between experiment and theory, the estimated spin values of bands L1, L3 and L4 were increased by $2-3\hbar$, i.e. within the limits allowed by the experimental data, with a corresponding increase of the excitation energies.

The neutron configuration calculated lowest in energy for $I = 38-54$ with three particles excited across the $N = 82$ gap, two in hf orbitals and one in the $i_{13/2}$ state, is assigned to the most intense band L1 while the L3 band is assigned to the next lowest band in this spin range with one hf and one $i_{13/2}$ particle. The low-spin extensions of bands L3 and L4, L3a and L4a, are assigned to the two signatures of the lowest energy configuration with no neutrons excited across the $N = 82$ gap. All these assignments results in a fair agreement between experiment and calculations, but, even so, they must be considered as tentative in view of of the freedom to adjust spin values and excitation energies of the observed bands.

The bandcrossing observed from L3a to L3 is suggested to occur via an intermediate configuration with only one hf and no $i_{13/2}$ neutrons. A reasonable interpretation of the bandcrossing from L4a to L4 is obtained if the connecting 1343-keV transition is assumed to be of electric dipole character. In that case, an excitation of a neutron from an $h_{11/2}$ to an $i_{13/2}$ orbital is assumed in the transition from the L4a to the L4 band. For the L2 band, it is proposed that its spin values should be decreased by $1\hbar$, in which case, its lower spin region might be assigned

to the next lowest configuration with no neutrons excited across the $N = 82$ gap while its less regular higher spin region appears to be even more uncertain.

VI. ACKNOWLEDGMENTS

A. Basu acknowledges the financial support from MHRD, Govt. of India. The authors are grateful to the ANL operations staff at Gammasphere. The help received from A.O. Macchiavelli, A. Bürger, and K. Juhász during the experiment is gratefully acknowledged. This work is supported by the German BMBF (06 BN 109), the Danish FNU Council for Natural Sciences, the National Research, Development and Innovation Fund of Hungary (Project No. K128947), the European Regional Development Fund (Contract No. GINOP-2.3.3-15-2016-00034), the U.S. Department of Energy, Office of Science, Office of Nuclear Physics, under contract Nos. DE-AC02-06CH11357 (ANL) and DE-AC02-05CH11231 (LBNL), and grants DE-FG02-97ER41041 (UNC), DE-FG02-97ER41033 (TUNL). This research used resources of ANL's ATLAS facility, which is a DOE Office of Science User Facility.

[1] S. Frauendorf and F.R. May, Phys. Lett B **125**, 245 (1983).
[2] Y.S. Chen, S. Frauendorf and G.A. Leander, Phys. Rev. C **28**, 2437 (1983).
[3] R. Wyss *et al.,* Nucl. Phys. A **505**, 337 (1989).
[4] A. Granderath *et al.*, Nucl. Phys. A **597**, 427 (1996).
[5] W. Lieberz *et al.,* Phys. Lett. B **240**, 38 (1990).
[6] A. K. Singh *et al.*, Phys. Rev. C **70**, 034315 (2004).
[7] A. Al-Khatib *et al.*, Phys. Rev. C **74**, 014305 (2006).
[8] A. Al-Khatib *et al.*, Eur. Phys. J. A **36**, 21 (2008).
[9] S. Nag *et al.*, Phys. Rev. C **88**, 044335 (2013).
[10] P. Singh, *et al.,* Phys. Rev. C **82**, 034301 (2010).
[11] P. Singh *et al.*, Phys. Rev. C **85**, 034319 (2012).
[12] P. Singh *et al.*, Phys. Rev. C **85**, 054311 (2012)
[13] S. Nag *et al.,* Phys. Rev. C **90**, 037302 (2014).
[14] J. Timár *et al.*, J. Phys. G **21**, 783 (1995).
[15] P. Singh, *et al.,* Phys. Rev. C **86**, 067305 (2012).
[16] P. Singh, *et al.,* Phys. Rev. C **84**, 024316 (2011).
[17] S. Nag *et al.,* Phys. Rev. C **94**, 034307 (2016).
[18] A. Al-Khatib *et al.,* Phys. Rev. C **83**, 024306 (2011).
[19] C. Rønn Hansen *et al.*, Phys. Rev. C **76**, 034311 (2007).
[20] A. Basu *et al.*, Phys. Rev. C **101**, 024309 (2020).
[21] I. Y. Lee, Nucl. Phys. A **520**, c641 (1990).
[22] D.C. Radford, Nucl. Instrum. Methods A **361**, 297 (1995).
[23] T. Bengtsson and I. Ragnarsson, Nucl. Phys. A **436**, 14 (1985).
[24] A.V. Afanasjev, D.B. Fossan, G.J. Lane, and I. Ragnarsson, Phys. Rep. **322**, 1 (1999)
[25] B. G. Carlsson and I. Ragnarsson, Phys. Rev. C **74**, 011302(R) (2006).
[26] B. G. Carlsson, I. Ragnarsson, R. Bengtsson, E. O. Lieder, R. M. Lieder, and A. A. Pasternak, Phys. Rev. C **78**, 034316 (2008).
[27] Hai-Liang Ma, B. Gillis Carlsson, Ingemar Ragnarsson, and Hans Ryde, Phys. Rev. C **90**, 014316 (2014).
[28] S. G. Nilsson and I. Ragnarsson, *Shapes and Shells in Nuclear Structure* (Cambridge University Press, Cambridge, England, 1995).
[29] V. M. Strutinsky, Nucl. Phys. A **122**, 1 (1968).
[30] G. Andersson *et al.*, Nucl. Phys. A **268**, 205 (1976).
[31] K. Pomorski and J. Dudek, Phys. Rev. C **67**, 044316 (2003).
[32] I. Ragnarsson, V.P. Janzen, D.B. Fossan, N.C. Schmeing and R. Wadsworth, Phys. Rev. Lett. **74**, 3935 (1995)
[33] T. Bengtsson, Nucl. Phys. A **496**, 56 (1989).